Planet. Sp. Sci., 45, 693, 1997

Pick-up ion dynamics at the structured quasi-perpendicular shock

D. Zilbersher and M. Gedalin

Department of Physics, Ben-Gurion University, P.O. Box 653, Beer-Sheva, 84105, Israel

Abstract

We study the pickup ion dynamics and mechanism of multiple reflection and acceleration at the structured quasi-perpendicular supercritical shock. The motion of the pickup ions in the shock is studied analytically and numerically using the test particle analysis in the model shock front. The analysis shows that slow pickup ions may be accelerated at the shock ramp to high energies. The maximum ion energy is determined by the fine structure of the electro-magnetic field at the shock ramp and decreases when the angle between magnetic field and shock normal decreases. Evolution of pickup ion distribution across the nearly-perpendicular shock and pickup ion spectrum is also studied by direct numerical analysis.

1 Introduction

Interstellar pickup ions play an important role in the physics of the outer heliosphere. They may modify both the large scale characteristics of the solar wind itself [1,2] and smaller scale solar wind structures such as interplanetary collisionless shock waves [3]. On the basis of the studies of the low-energy cosmic rays it was proposed that the cosmic ray anomalous component originates from the interstellar pickup ions, accelerated at the quasi-perpendicular shocks [4,5].

The observations, made by Ulysses at 4.5AU [6], have revealed accelerated interstellar pickup ions across the forward shock in the corotating interaction regions. It has been found that the injection efficiency for these pickup ions exceeds that one for solar wind ions, and that the accelerated pickup ions have power-law energetic spectra in the solar wind frame [6]. Earlier investigations of the quasi-perpendicular cometary bow shocks have observed water-group pickup ions with speeds of several times the solar wind speed v_u at and downstream of the shock[7,8].

Process of pickup ions production and features of the pickup ion distribution in the solar wind are studied quite well. Neutral atoms and molecules, penetrating from

the local interstellar medium or escaping from comets, are ionized by photoionization, electron impact or charge exchange with the solar wind. Under influence of the solar wind electro-magnetic field the ions compose ring-beam distribution in velocity space. Then they are scattered by ambient and excited Alfvenic fluctuations to form spherical shell distribution, centered approximately at the solar wind velocity with a radius of about solar wind speed V_u [9,10].

Accelerated pickup ions were observed at quasi-perpendicular shocks, which are not able to accelerate incident thermal ions and pick up ions by the standard diffusive shock (Fermi) acceleration mechanism [11]. The mechanism requires ions which can penetrate the shock front in both directions. At quasi-perpendicular shocks it may occur when the ion velocity near the shock ramp is higher than a definite threshold speed, which significantly exceeds the solar wind speed [11,12]. Hence, in order that pick up ions may be accelerated by the diffusive mechanisms, some preacceleration mechanism at quasi-perpendicular shocks must exist. In [3], a detailed discussion was presented of the following idea for the ion acceleration at a perpendicular shock proposed by [13]: if the ion encounters the shock with normal kinetic energy $m_i v_n^2/2$ much smaller than the electrostatic potential $e\varphi_0$ at the shock, and the upstream Lorentz force is directed toward the shock, then the ion finds itself trapped between the shock potential and the Lorentz force. Such ion is multiply reflected at the shock front and during each excursion to the upstream region it gains some energy until it is able to overcome the shock, when $m_i v_n^2/2 > e\varphi_0$ or the Lorentz force in the normal direction exceeds the electrostatic force in the ramp. This idea for pickup ion preacceleration at the quasi-perpendicular shock has been developed further by several authors. Analytical estimates show that at the perpendicular shock the maximum energy gain for transmitted ions is proportional to the ratio of an solar wind ion gyroradius to the smallest characteristic scale of the electrostatic potential [3]. At the quasi-perpendicular shock maximum energy gain occurs when the ion escapes back into the upstream region [14]. The multiple reflection ion acceleration gives very hard power law spectrum [3]. The spectrum is weakly sensitive to the shock parameters and may extend to energy ~ 0.5MeV. Thus the injection problem associated with Fermi acceleration probably, may be solved by the multiple reflection ion acceleration mechanism.

In the present paper we study the details of the multiple reflected ion acceleration mechanism in the stationary structured quasi-perpendicular supercritical shock and determine the shock parameters, which control the pickup ion energy gain. We also consider evolution of the pickup ion distribution across the strong shock. Our approach differs from earlier ones in that we use field models qualitatively describing the actual structure of the stationary fields at quasi-perpendicular super-critical shocks which consists of the extended foot, narrow ramp, overshoot and downstream region. In section 2 we consider analytically the pickup ion motion at the shock front and derive the multiple reflection condition as a function of the field parameters. In section 3 we numerically analyze the ion motion in the stationary

model shock front. The analysis illustrates the analytical consideration of multiple reflection process developed in section 2 and provides additional information about the process. The method also allows diagnostics of pickup ion distribution at the shock and of pickup ion spectra before the ramp and in the far upstream and downstream regions.

2 Pickup ion dynamics in the shock front

When studying the pickup ion dynamics in the shock front we adopt the usual assumptions that the shock is one-dimensional and stationary. In doing so we do not consider the effects of, for example, possible rippling of the shock surface or interaction with waves, assuming that the stationary electric and magnetic fields in the shock front determine the ion behavior (see, however, discussion in sec. 4).

We shall work in the normal incidence frame (N), where the upstream plasma velocity is along the shock normal. Let us choose the coordinates in such a way that the normal is along x axis which is directed toward the downstream region (in [14] x axis was directed toward the upstream region), upstream and downstream magnetic fields are in xz plane, and the noncoplanarity direction is along y axis. Then the ion motion is governed by the following equations of motion:

$$m_i \dot{v}_x = e(E_x + v_y B_z - v_z B_y), \tag{1}$$
$$m_i \dot{v}_y = e(E_y + v_z B_x - v_x B_z), \tag{2}$$
$$m_i \dot{v}_z = e(v_x B_y - v_y B_x), \tag{3}$$

where B_y, B_z, and $E_x = -d\phi/dx$ depend only on x, while $B_x = \text{const}$, and the motional electric field $E_y = V_u B_u \sin\theta = \text{const}$ (where V_u is the upstream flow speed). Here subscript u denotes asymptotically homogeneous upstream parameters, and θ is the angle between the shock normal and upstream magnetic field vector.

The qualitative profile of the magnetic field is known quite well. It is usually considered [15] to consist of the extended foot with $L_f \sim 0.5(V_u/\Omega_u)$ (where $\Omega_u = eB_u/m_i$ is the upstream ion gyrofrequency), on which the magnetic field B_z gradually increases by the amount of $\lesssim B_u$. It is followed by the narrow ramp with the width $c/\omega_{pi} > L_r > c/\omega_{pe}$, where the main magnetic field B_z jump occurs, and magnetic overshoot and probably large downstream magnetic field oscillations. The noncoplanar magnetic field component B_y is always small relative to B_z, and negligible upstream. Substantial component of pickup ions may affect the shock profile and alter the typical scales (see detail discussion in [3]). Here we consider pickup ions as a low density test particle population.

The electric field profile is known much worse. It is distributed over the whole

shock front including foot, ramp, and overshoot, and penetrates into the downstream region, so that only a part of the total cross-shock potential is applied at the ramp.The qualitative picture of the quasi-perpendicular shock front is shown in Figure 1.

An ion with a low kinetic energy in x direction ($m_i v_x^2/2 << e\phi$) is unable to overcome the electrostatic potential at the ramp and is reflected back to the upstream region. If $v_y B_z > 0$, upstream Lorentz force returns it to the ramp again. In this way the ion becomes trapped near the ramp and quickly oscillates in x direction until it escapes upstream or downstream region [3,14].

It does not seem possible to solve (and even analyze quantitatively) the ion equations of motion (1)-(3) in the general case of Figure 1. Instead we shall analyze them for the case of surfing ions, which are assumed to be trapped in the ramp vicinity. To do so we make an assumption (verified aposteriori) that these ions oscillate quickly in x direction, while two other velocity components vary slowly on the oscillation period (such behavior can be expected since strong ion acceleration is possible only when E_y acts on the ion for a substantially long time). In this case separating fast and slow motion, one has:

$$m_i \dot{v}_x = -e\frac{d\phi_{\text{eff}}}{dx}, \tag{4}$$

$$m_i \dot{v}_y = e(E_y + v_z B_x), \tag{5}$$

$$m_i \dot{v}_z = -e v_y B_x, \tag{6}$$

where (4) describes fast oscillations along x, while (5) and (6) describe slow motion in yz plane. The effective potential

$$\phi_{\text{eff}} = \phi - v_y A_y - v_z A_z, \tag{7}$$

$$B_z = \frac{dA_y}{dx}, \qquad B_y = -\frac{dA_z}{dx}, \tag{8}$$

weakly depends on time via slow time-dependence of v_y and v_z. Further simplification can be achieved by consideration a model profile, where $\mathbf{B} = \mathbf{B}_u$ and $\mathbf{E} = (0, E_y, 0)$ before the ramp, and Taylor expanding up to the first order

$$B_y = (\frac{dB_y}{dx})|_{x=0} x, \tag{9}$$

$$B_z = B_u \sin\theta + (\frac{dB_z}{dx})|_{x=0} x, \tag{10}$$

$$E_x = (\frac{dE_x}{dx})|_{x=0} x, \tag{11}$$

in the vicinity $x > 0$ of the upstream edge of the ramp ($x \to -\infty$ and $x \to +\infty$ corresponds to the asymptotically homogeneous upstream and downstream regions, respectively). This approach implicitly assumes that the trapped ions do not penetrate the ramp deeply. In this case the effective potential takes the following

form

$$\phi_{\text{eff}} = \begin{cases} -v_y B_u \sin\theta x, & x < 0, \\ \frac{1}{2}\lambda x^2 - v_y B_u \sin\theta x, & x > 0 \end{cases} \tag{12}$$

where

$$\lambda = -\frac{dE_x}{dx} - v_y \frac{dB_z}{dx} + v_z \frac{dB_y}{dx}, \tag{13}$$

where the derivatives are taken at $x = 0$, and $\phi_{\text{eff}} = 0$ at the upstream edge of the ramp $x = 0$.

Estimating typical $dE_x/dx \sim \Delta\phi/L_r^2 \sim 0.5 m_i V_u^2/2eL_r^2$ and $dB_z/dx \sim \Delta B_z/L_r \sim B_u/L_r$, where L_r is the ramp width, one finds that the term dE_x/dx in λ dominates unless $v_y/V_u \gtrsim (V_u/\Omega_u)/L_r = M_A(c/\omega_{pi})/L_r$, where M_A is Alfven Mach number.

Equations (4) and (12) describe oscillations in a potential well (if $\lambda > 0$, which is typical for the quasiperpendicular shock front), with the potential minimum of $\phi_{\text{min}} = -(v_y B_u \sin\theta)^2/2\lambda$ at $x = v_y B_u \sin\theta/\lambda$. The equations of motion are easily solved as follows.

In the region $x < 0$ one has (the initial condition is $v_x = v_{x0}$ - x-component of the reflected ion velocity before its excursion to the upstream region, $x = 0$):

$$v_x^2 = v_{x0}^2 + 2v_y\Omega_u x, \tag{14}$$

while in the region $x > 0$ the solution has the following form:

$$x = x_m + \Delta\sin(\omega t - \varphi_0), \tag{15}$$

$$v_x = \omega\Delta\cos(\omega t - \varphi_0), \tag{16}$$

$$\varphi_0 = \arcsin\frac{\beta}{(\beta^2 + \lambda m_i v_{x0}^2/e)^{1/2}}, \tag{17}$$

$$\omega = (e\lambda/m_i)^{1/2}, \quad \beta = v_y B_u, \quad x_m = \beta/\lambda, \quad \Delta = \frac{(\beta^2 + \lambda m_i v_{x0}^2/e)^{1/2}}{\lambda}, \tag{18}$$

where v_{x0} is a slowly varying function of time.

When v_y and v_z vary slowly, the integral $\oint pdq = \oint m_i v_x dx$ over a closed trajectory is adiabatically invariant. Direct calculation gives

$$I = I_1 + I_2, \quad I_1 = \oint_{x<0} m v_x dx, \quad I_2 = \oint_{x>0} m v_x dx, \tag{19}$$

$$I_1 = \frac{1}{3} m_i^2 \frac{v_{x0}^3}{\beta}, \tag{20}$$

$$I_2 = \frac{m_i\omega}{\lambda^2}(\beta^2 + \lambda m_i v_{x0}^2/e)[\frac{\pi}{2} + \arcsin\frac{\beta}{(\beta^2 + \lambda m_i v_{x0}^2/e)^{1/2}} - \frac{1}{2}\frac{\lambda m_i v_{x0}}{(\beta^2 + \lambda m_i v_{x0}^2/e)^{1/2}}] = \text{const}. \tag{21}$$

It is easy to analyze the consequences in the limiting cases. If $\lambda m_i v_{x0}^2/\beta^2 \ll 1$ (very low initial velocities at the upstream edge of the ramp), $I_2 \gg I_1$ and

$$I_2 \approx \frac{\pi\beta^2}{\lambda^{3/2} m_i^{1/2}} = \text{const}, \tag{22}$$

which corresponds actually to the case $v_{x0} \to 0$. In the opposite limit $\lambda m_i v_0^2/\beta^2 \gg 1$ the upstream part dominates $I_1 \gg I_2$ and

$$I_1 \approx \frac{m_i^2 v_{x0}^3}{\beta} = \text{const}, \tag{23}$$

which immediately gives $v_{x0} \propto v_y^{1/3}$ [14].

Maximum kinetic energy of the oscillations is determined by the energy conservation:

$$(\frac{m_i v_x^2}{2})_{\text{max}} = \frac{m_i v_{x0}^2}{2} + (v_y B_u \sin\theta)^2/2\lambda, \tag{24}$$

and remains relatively small with the dependence weaker than $v_x \propto v_y$.

Roughly estimating, the ion trapping ceases and it is transmitted downstream if it crosses the middle of the ramp. Hence the additional trapping condition is $m_i v_{x0}^2/2 < e\phi(x = L_r/2)$, or

$$\frac{m_i v_0^2}{2}(\frac{v_y}{v_{y0}})^{2/3} + \frac{v_y B_u L_r}{2} < \frac{e\phi}{2}, \tag{25}$$

where v_0 is the initial ion x velocity, v_{y0} is its initial y velocity, and ϕ is the cross-ramp potential. Taking into account that v_0 is small and assuming that dE_x/dx is the dominant contribution in λ, one finds the following estimate for the maximum v_y during the trapping:

$$(v_y)_{\text{max}}^{(\text{trap})} = \frac{e\phi}{B_u L_r} - \frac{m_i v_0^2}{B_u L_r}\left(\frac{e\phi}{B_u L_r v_{y0}}\right)^{1/3}. \tag{26}$$

The second term in the last equation is a correction to the step function based estimate for $(v_y)_{\text{max}}$ [3].

On the other hand, the solution of the slow equations with the initial condition $v_y = v_{y0}$, $v_z = v_{z0}$ is

$$v_y = v_{y0}\cos(\Omega_u \cos\theta t) + (v_{z0} + V_u \tan\theta)\sin(\Omega_u \cos\theta t), \tag{27}$$
$$v_z = (v_{z0} + V_u \tan\theta)\cos(\Omega_u \cos\theta t) - v_{y0}\sin(\Omega_u \cos\theta t) - V_u \tan\theta, \tag{28}$$

and

$$(v_y)_{\text{max}}^{(\text{slow})} = [v_{y0}^2 + (v_{z0} + V_u \tan\theta)^2]^{1/2}. \tag{29}$$

If $(v_y)_{\max}^{(\text{slow})} < (v_y)_{\max}^{(\text{trap})}$, the ion is not transmitted downstream but remains trapped and its v_y and v_x decrease until it escapes upstream.

It is difficult to determine precisely the moment when the ion escapes upstream. We shall estimate the escape conditions assuming that the escape itself occurs when $|v_x|$ and v_y come back (decrease again) to their initial values. In that case v_z can be easily determined using energy conservation in the de Hoffman-Teller frame (HT, in which the plasma upstream velocity is along the upstream magnetic field). The transformation rule between the two frames is

$$v_x^{(N)} = v_x^{(HT)}, \quad v_y^{(N)} = v_y^{(HT)}, \tag{30}$$

$$v_z^{(N)} = v_z^{(HT)} - V_u \tan\theta. \tag{31}$$

Since E_x is negligible upstream, the total HT potential is zero in this region and energy conservation gives $(\mathbf{v}^{(HT)})^2 = \text{const}$, which in our case results in the following estimate of the escape velocity:

$$v_z^{(N,\text{escape})} = -v_{z0}^{(N)} - 2V_u \tan\theta. \tag{32}$$

It is worth mentioning that in this picture the ions experience reflection in which their noncoplanar velocity v_x does not change, while others (v_x and v_z) change their sign in HT.

It should be mentioned that the above analysis is approximate (since the shock profile is treated in a specific model) and applies only to those ions which are trapped and subsequently either transmit downstream and do not appear at the ramp anymore or escape upstream. The analysis is not able to catch trajectories which do not meet these assumptions and we have to consider them numerically in the next section. We also do not consider here the ions which experience the shock drift acceleration (cf. [3]).

3 Numerical analysis.

In order to illustrate the above theoretical analysis and study the features, which cannot be studied analytically, we perform a test particle numerical analysis of pickup ion trajectories in a model shock front, which is taken to resemble the observed shock profiles, as in Figure 1. The corresponding model analytical form for

the fields is taken as proposed by [16]:

$$B_x = B_u \cos\theta = \text{const}, \tag{33}$$

$$B_y(x) = \frac{cB_x}{4\pi neV_u}\frac{dB_z(x)}{dx}, \tag{34}$$

$$B_z(x) = B_u \sin\theta(1+$$
$$\frac{R_f-1}{2}(1+\tanh\frac{3(x+D_f-3D_r)}{D_f}) + \frac{R_r-R_f}{2}(1+\tanh\frac{3x}{D_r})$$
$$+ (R_o-R_r)\exp(-\frac{2(x-D_o)^2}{D_o^2})$$
$$+ \frac{R_d-R_r}{2}(1+\tanh\frac{3(x-D_o-D_d)}{D_d}), \tag{35}$$

$$E_x(x) = -\frac{1}{ne}\frac{dp_{e,xx}}{dx} - \frac{1}{8\pi ne}\frac{dB_z^2}{dx} - \frac{\phi}{\sqrt{\pi}d_e}\exp(-\frac{x^2}{d_e^2}) \tag{36}$$

$$E_y = \frac{\mathbf{V_u}\times\mathbf{B_u}}{c} = \text{const}, E_z = 0. \tag{37}$$

where d_e is the scale of the additional Gaussian electric field variation, D_f, D_r and D_o control the foot, ramp and overshoot thicknesses respectively, $p_{e,xx} \propto n^{\gamma_e}$, $n \sim B_z$. The suggested form of B_z describes qualitatively the front structure: foot at $-D_f < x < -D_r/2$, ramp $-D_r/2 < x < D_r/2$, and overshoot $D_r/2 < x < (D_o + D_d)$ (it should be noted that here for convenience $x = 0$ corresponds to the middle of the ramp). The noncoplanar component B_y is in agreement with the results of [17,18]. The suggested analytical profile of the cross-shock electric field consists of the well-known hydrodynamical part (first two terms) for polytropic electrons, and additional Gaussian to take into account the penetration of the field in deep downstream and foot and provide the observed values of the total cross-shock potential drop. For the specific needs of the present paper the parameters were chosen as follows: $R_f = 1.5$, $R_r = 5$, $R_o = 6$, $R_d = 3.2$, $D_f = 0.3(V_u/\Omega_u)$, $D_r = 0.01(V_u/\Omega_u)$ (this parameter was varied, see below), $D_o = 0.1(V_u/\Omega_u)$, $D_d = 0.15(V_u/\Omega_u)$, and $\gamma_e = 2$. We chose to examine a high-Mach number $M_A = 7.5$.

The initial pickup ion distribution was assumed to be the following shell distribution [19,20,]

$$f(\mathbf{v}) = \frac{n_0}{4\pi V_u^2}\delta(|\mathbf{v}-\mathbf{V_u}| - V_u). \tag{38}$$

at the upstream edge of the foot.

Pickup ion trajectories are traced through the described shock front starting at the upstream edge of the foot $x = -D_f$. Figure 2 presents the ion trajectories projected onto the xy-plane at the quasi-perpendicular shock with $\theta = 70°$. A variety of pickup ion trajectories are seen: 1) ions which are directly transmitted downstream, 2) ions which cross the ramp from downstream to upstream once or several times, 3) ions which are reflected in the ramp only once, 4) ions which are accel-

erated by multiple reflection mechanism and then escape either to downstream or to upstream, and 5) multiply reflected ions which rotate around the ramp until they escape upstream.

Next several figures provide more qualitative details about the multiple reflection (trapping) process.Figure 3 shows the trajectory of an ion which is transmitted downstream after several reflections. It is seen that at each next encounter with the ramp the ion penetrates into the ramp more deeply, while both v_x and v_y increase, until the ion crosses the ramp at the maximum of v_y and drifts downstream having a high gyration velocity. The initial ion energy is about $m_i V_u^2/2$, and it is accelerated to about four times higher downstream energy in four cycles of reflection.

Figure 4 shows the trajectory of an ion which escapes upstream after making a full cycle of multiple reflections, during which v_y increases and decreases again. Figure 4a shows that the ion trajectory does not cross the middle of the ramp. From Figure 4b one can see that the amplitude of oscillations of v_x is roughly proportional to v_y, that is, the adiabatic approximation works quite well. It is seen also that the reflection-escape process is indeed almost specular in $v_x - v_y$ plane: v_y is the same at the entry and escape points, while v_x changes its sign. As can be seen from Figure 4c, v_z in the last escape point closely corresponds to (32).

Figure 5 shows the trajectory which is not covered by the above theoretical analysis. The ion is trapped near the ramp for some time and afterwards it becomes trapped around the ramp, making several large amplitude gyrations and crossing the shock front back and forth. Eventually it escapes upstream (high negative final v_z in Figure 5c) having a substantial gyration velocity.

Figure 6a shows which part of the initial pickup ion distribution undergoes multiple reflection (for perpendicular shock geometry). In Figure 6b we show the same distribution of incident pickup ions at the upstream edge of the ramp, where it is already strongly disturbed. Almost all multiply reflected ions are taken from the low v_x part of the distribution, in agreement with previous theoretical observations [3,14]. Most of them have substantial positive v_y at their entry to the ramp, as is expected according to the analytical consideration.

The next several figures present the evolution of the pickup ion distribution across the structured shock front. In Figure 7 we present the pickup ion distributions obtained numerically by tracing the initial shell distribution (38) across the perpendicular shock. The distributions are plotted for several positions: (a) before the foot at $x = -0.6(V_u/\Omega_u)$, (b) at the upstream edge of the ramp $x = -0.005(V_u/\Omega_u)$, (c) at the downstream edge of the ramp $x = 0.005(V_u/\Omega_u)$, and (d) far downstream at $x = 5(V_u/\Omega_u)$. The ion distribution before the foot (Figure 7a) consists of the incident pickup ion shell and ions which are reflected in the way similar to the reflection of the ions from the wings of the thermal ion distribution [16]. The ion distribution at the upstream edge of the ramp (Figure 7b) includes these reflected

ions and much more energetic trapped accelerated ions, which are seen also just behind the ramp in Figure 7c (only those which crossed the ramp and are transmitted further downstream). Far downstream distribution (Figure 7d) consists of low energy reflected ions and high energy multiply reflected ones. Since there is not gyrophase mixing in the perpendicular shock (all ions have the same downstream drift velocity) the downstream distribution is spatially dependent (actually periodic).

Figure 8 present the evolution of pick up ion distribution across the nearly perpendicular $\theta = 80^\circ$ shock. For each position both v_x, v_y and v_y, v_z projections are shown. The distribution before the foot (Figures 8a and 8b) differs from that one in the perpendicular case (Figure 7a) only by presence of ions which escaped upstream (high negative v_z). The upstream edge distribution (Figures 8c and 8d) also shows presence of these escaping ions. The multiply reflected ions in Figure 8d lie on two semicircles, corresponding to the slow rotation in v_y, v_z plane (see (5) and (6)), separately for positive and negative initial v_z. The most remarkable difference from the perpendicular case can be seen in the downstream distribution (Figures 8g and 8h), which shows strong phase mixing. The downstream accelerated pickup ions are situated on two (almost) hemispheres, corresponding to the rotation of the semi-circles in Figure 8f.

The numerical analysis allows also to obtain the differential energy spectra of accelerated ions. Figure 9 shows the far upstream (Figure 9a) and far downstream (Figure 9b) ion energy spectra $dN/d\epsilon$,

$$\frac{dN}{d\epsilon} = \frac{m_i V_u^2}{2} \frac{v}{m_i} \int f(v, \theta, \varphi) \sin\theta d\theta d\varphi \tag{39}$$

where ϵ is the dimensionless ion energy, $\epsilon = (m_i v^2/2)/(m_i V_u^2/2)$. The far upstream spectrum consists of the dense population of incident ions ($dN/d\epsilon = \text{const}$) and low density high energy component of accelerated ions which escaped upstream for two different angles between the shock normal: $\theta = 80^\circ$ (dotted line) and $\theta = 70^\circ$ (dashed line). With the decrease of the angle the number of escape ions (Figure 9a) increases but their energy decreases. One can see also the drastic drop of acceleration efficiency with the increase of obliquity in the downstream distribution of pickup ions, where the highest energy of accelerated ions drops from 10^2 (in $m_i V_u^2/2$) to slightly higher than 10^1 when the angle decreases from 80° to 70°.

Figure 10 shows the accelerated pickup ion distribution just before the ramp and far downstream for two values of the total cross-shock potential. As could be expected, the acceleration efficiency decreases with the decrease of the potential, although this decrease is almost not noticeable in the far downstream distribution because of the logarithmic scale. It is clearly seen that the distribution is nearly exponential $dN/d\epsilon \propto \exp(-\alpha\epsilon)$ at the upstream edge of the ramp, with $\alpha \approx 0.020$ for the potential $\varphi = 0.7(m_i V_u^2/2)$, and $\alpha \approx 0.033$ for $\varphi = 0.5(m_i V_u^2/2)$. The downstream distributions reveal power spectra $dN/d\epsilon \propto \epsilon^{-\beta}$, where $\beta \approx 3/2$ and is almost in-

dependent of the cross-shock potential. The result is in conformity with the power low tail in energy produced by multiply reflected ion acceleration at strong perpendicular shock found in [3].

Dependence of the accelerated ion spectra on the ramp width is shown in Figure 11, where the upstream-ramp-edge and far downstream spectra are presented for the ramp width $D_r = 0.01(V_u/\Omega_u)$ (solid line) and $D_r = 0.03(V_u/\Omega_u)$ (dotted line). As is expected, the acceleration efficiency drops drastically when the sock becomes wider. It could be expected, however, that any substructure in the ramp would enhance the acceleration, as can be seen from Figure 12, where the ion spectra are compared for the case of $D_r = 0.03(V_u/\Omega_u)$ without (dotted line) and with a substructure (dashed line). Presence of such internal substructure plays the role of a narrow ramp.

It is worth to mention that our approach allows also to study the behavior of heavy ions. Figure 13 presents the results of such analysis, comparing the downstream spectra of ions with the mass $m_i = 4m_p$ (which would correspond to He^+ ions) and $m_i = 15m_p$ (O^+). The initial distribution is the same pickup ion shell as for the case $m_i = m_p$, considered throughout the paper. It can be seen that the acceleration is less efficient for heavy ions than for protons (Figures 9b and 10b). Detailed analysis of the heavy ion behavior is beyond the scope of the present paper and will be presented elsewhere.

4 Conclusions

We have considered the surfing mechanism of the pickup ion energization at strong high-Mach number quasi-perpendicular shocks. The distribution of the electromagnetic field at the shock front determines the ion motion across the shock,and the ion reflection and acceleration processes depend on the details of the fine structure of the shock front. We had to make a choice of the shock structure in order to determine quantitatively the features of the accelerated ions and their dependence on the shock parameters. It is clear that a deviation of the actual shock structure from the model adopted here would give somewhat different quantitative results, which cannot be predicted unless we know profiles of the fields at the shock. However, some tendencies can be predicted on the basis of the analytical and numerical investigations represented in sections 2 and 3.

The conditions for the multiple ion reflection and the maximum energy gain are determined by the slope of the electric and magnetic field profiles at the ramp and therefore very sensitive to the ramp width. For the chosen model the scales of the magnetic and electric field variations are the same and $\approx D_r$. The analytical consideration gives the following estimate for the maximum downstream ion energy in

the nearly perpendicular shock (see also [14,3]):

$$\mathcal{E}_{\max} \approx \frac{m_i V_u^2}{2} (\frac{2\phi}{D_r R})^2, \tag{40}$$

where $\phi = e\varphi/(m_i V_u^2/2)$, $R = B_{zr}/B_u$ (where B_{zr} is z component of the magnetic field at the downstream edge of the ramp), and D_r is measured in V_u/Ω_u. For the initial ion energy of $\mathcal{E} = 1$keV, ramp width of $D_r \approx 0.01(V_u/\Omega_u)$, cross-shock potential $\phi = 0.5$, and magnetic compression ratio $R = 2.5$, one finds $\mathcal{E}_{\max} \approx 1$MeV, which is probably sufficient for injection into diffusive acceleration regime.

Since the efficiency is $\propto D_r^{-2}$ and decreases with the increase of obliquity, the pick up ion injection for Fermi acceleration mechanism seems to be effective only at nearly-perpendicular shocks waves with very narrow ramp or when some substructure is present which reduced the effective width of the ramp.

The dependence of the acceleration features on the Mach number is determined mostly by the dependence of the shock width and magnetic compression ratio on the Mach number. In the absence of a satisfactory theory, which could provide these dependencies, the only conclusion is that the mechanism efficiency should rapidly decrease with the decrease of the Mach number because of the shock widening.

The obtained model downstream accelerated ion spectra $\propto \epsilon^{-3/2}$ (see also [3]), which corresponds to $f(v) \propto v^{-2}$ (and is in agreement with earlier studies), is harder than v^{-4} that is observed. This discrepancy may be probably attributed to the mentioned deviation of the actual shock structure from the adopted model.

It should be mentioned that, due to the high sensitivity of the trapping-detrapping mechanisms to the details of the magnetic and electric fields in the ramp, it could be in principle affected by even relatively weak deviations from stationarity (for example, presence of large amplitude waves in the ramp) or one-dimensionality (like rippling of the shock surface), as well as presence of any small-scale substructure inside the ramp. Observation evidence is not unambiguous, and the effect of such deviations from the model is not clear apriori and requires special study which is beyond the scope of the present paper.

In summary, the analysis allowed to shed additional light on the importance of the small-scale structure of the shock front (in particular, high gradients of the electric field) for the ion acceleration processes. The test particle numerical analysis allowed to determine the details of ion behavior and the spatial and energetical distribution of accelerated ions in the shock front.

This research was partially supported by grant 94-00047 from the United States-Israel Binational Science Foundation (BSF), Jerusalem, Israel and partially by THE ISRAEL SCIENCE FOUNDATION founded by The Israel Academy of Sciences and Humanities.

References

[1] T.E. Holzer,Interaction of the solar wind with the neutral component of the interstellar gas, *J.Geophys.Res.*, **77** (1972) 5407-5431.

[2] P.A. Isenberg, Interaction of the solar wind with interstellar neutral hydrogen: three fluid model, *J. Geophys.Res.*, **91** (1986) 9965-9972.

[3] G.P. Zank, H.L. Pauls, I.H. Cairns, G.M. Webb, Interstellar pick-up ions and quasi-perpendicular Shocks: Implications for the Termination Shock and interplanetary shocks, *J. Geophys.Res.*, **101** (1996) 457-478.

[4] L.A. Fisk, B. Kozlovsky, and R. Ramaty, An interpretation of the observed oxygen and nitrogen enhancements in low-energy cosmic rays,*Astrophys.J.*, **190** (1974) L35-37.

[5] J.R. Jokipii, Particle acceleration at a termination shock, 1. Application to the solar wind and the anomalous component, *J.Geophys.Res.*, **91** (1986) 2929-2932.

[6] G. Gloeckler, J. Geiss, E.C. Roelof, L.A. Fisk, F.M. Ipavich, K.W. Ogilvie, L.J. Lanzerotti, R. von Steiger, and B. Wilken, Acceleration of interstellar pickup ions in the disturbed solar wind observed on Ulysses, *J.Geophys.Res.*, **99** (1994) 17637-17643.

[7] F.M. Ipavich, A.B. Galvin, G. Gloeckler, D. Hovestadt, B. Klecker, and M. Scholer, Comet Giacobini-Zinner: In situ observation of energetic heavy ions, *Science*, **232** (1986) 366-369.

[8] A.J. Coates, A.D. Johnstone, B. Wilken, K. Jockers, and K.-H. Glassmeier, Velocity space diffusion of pick up ions from the water group at comet Halley, *J.Geophys.Res.*, **94** (1989) 9983-9993.

[9] R.Z. Sagdeev, V.D. Shapiro, V.I. Shevchenco, and K. Szego, MHD turbulence in the solar wind-comet interaction region, *Geophys.Res.Lett.*, **13** (1986) 85-88.

[10] M.A. Lee, and W.-H. Ip, Hydromagnetic wave excitation by ionized interstellar hydrogen and helium in the solar wind, *J.Geophys.Res.*, **92** (1987) 11,041-11,052.

[11] G.M. Webb, G.P. Zank, C.-M. Ko, and D.J. Donohue, Multi-dimensional Green's functions and the statistics of diffusive shock acceleration, *Astrophys.J.*, **453** (1995) 178-206.

[12] J.R. Jokipii, Constraints on the acceleration of anomalous cosmic rays, *Astrophys.J.Lett.*, **393** (1992) L41-43.

[13] R.Z. Sagdeev, Cooperative phenomena and shock waves in collisionless plasma, in: *Reviews of Plasma Physics*, ed. M.A.Leontovich, Vol.4 p.23, (Consultants Bureau, New York, 1966).

[14] M.A. Lee, V.D. Shapiro and R.Z. Sagdeev, Pick-up ion energization by shock surfing, *J.Geophys.Res.*, **101** (1996) 4777-4790.

[15] J.D. Scudder, A. Mangeney, C. Lacombe, C.C. Harvey, T.L. Aggson, R.R. Anderson, J.T. Gosling, G. Paschmann, and C.T. Russell, The resolved layer of a collisionless, high β, supercritical, quasi-perpendicular shock wave, 1, Rankine-Hugoniot geometry, currents, and stationarity, *J.Geophys.Res.* **91** (1986) 11,019-11,052.

[16] M. Gedalin, Ion reflection at the shock front revisited, *J. Geophys. Res.*, **101** (1996) 4871-4878.

[17] F.C. Jones, and D.C. Ellison, Noncoplanar magnetic fields, shock potentials, and ion deflection, *J.Geophys.Res.*, **92** (1987) 11,205-11,207.

[18] M. Gedalin, Noncoplanar magnetic field in the collisionless shock front, *J. Geophys. Res.*, **101** (1996) 11,153-11,156.

[19] P.C. Liewer, B.E. Goldstein and N. Omidi, Hybrid simulations of the effects of interstellar pickup hydrogen on the solar wind termination shock, *J.Geophys.Res.*, **98** (1993) 15,211-15,220.

[20] J. Giacalone, J.R. Jokipii and J. Kota, Ion injection and acceleration at quasi-perpendicular shocks, *J.Geophys.Res.*, **99** (1994) 19,351-19,358.

Figures and Figure captions

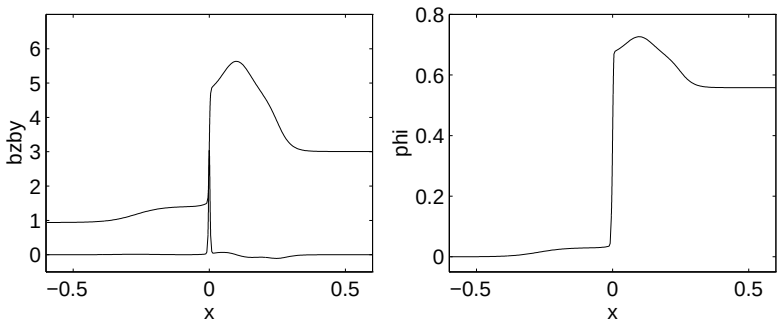

(a) (b)

Fig. 1. The (a) magnetic field and (b) electric potential profiles in the high-Mach number quasi-perpendicular shock.

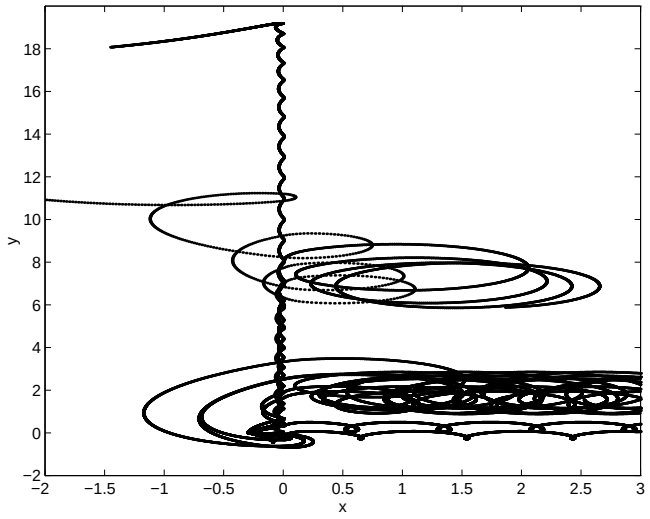

Fig. 2. Trajectories of 20 ions at the high-Mach number supercritical quasi-perpendicular $\theta = 70^\circ$ shock.

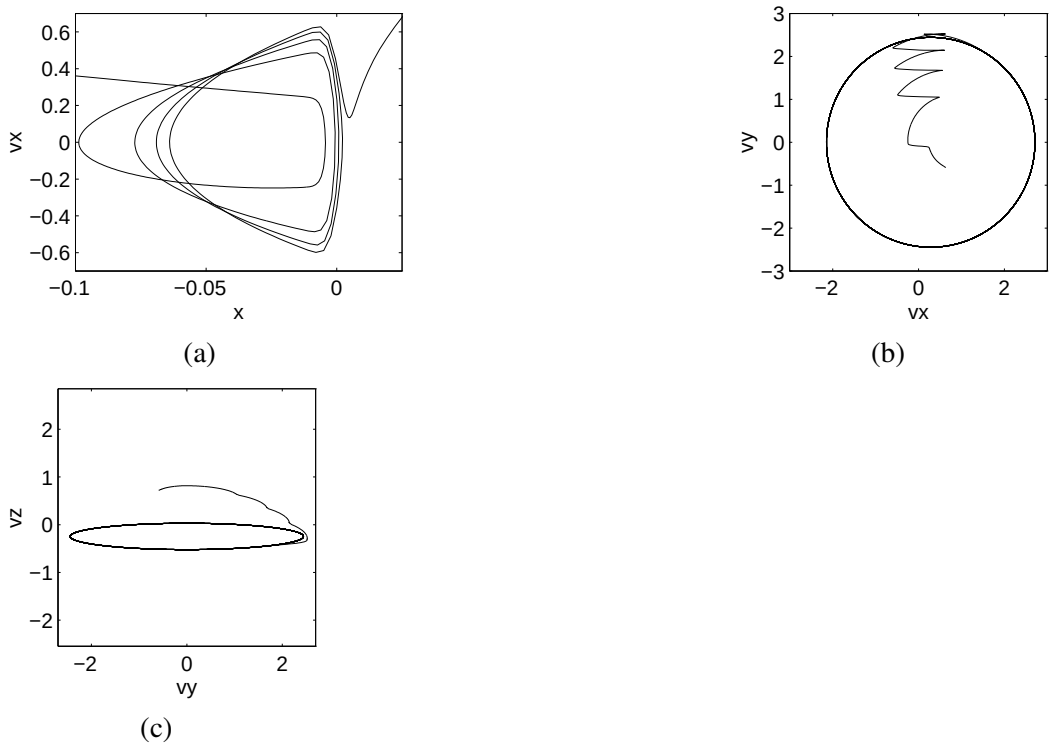

Fig. 3. Trajectory of a multiply reflected ion escaping downstream.

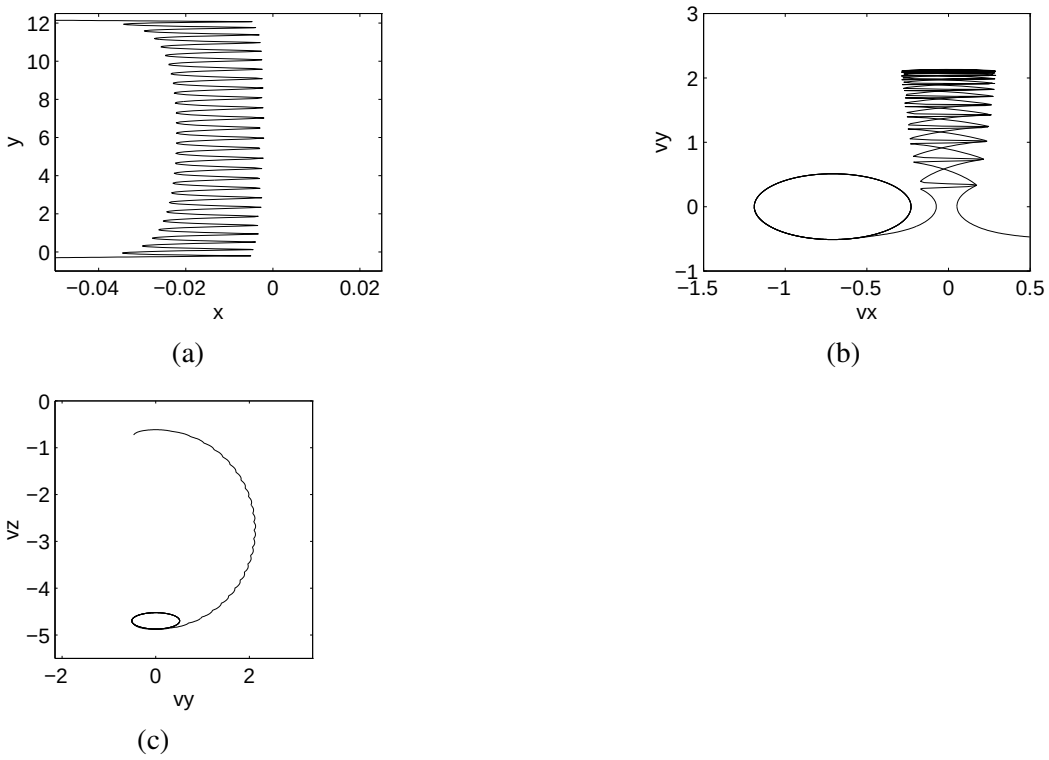

Fig. 4. Trajectory of a trapped ion which, after multiple reflection, escapes upstream.

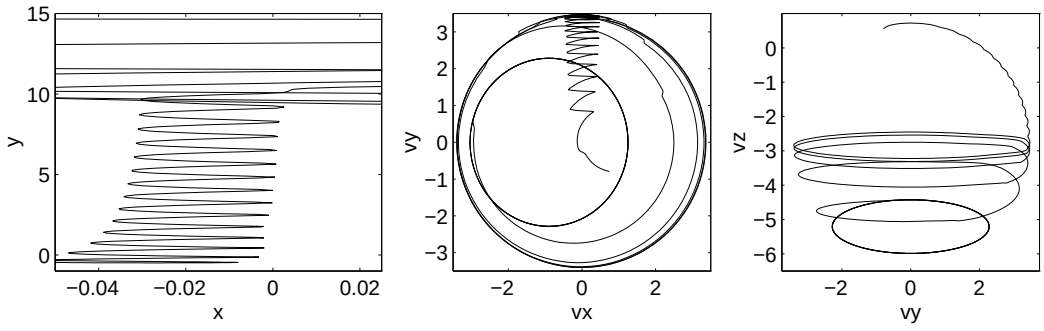

(a) (b) (c)

Fig. 5. Trajectory of a trapped ion which, after multiple reflection, rotates around the ramp until it escapes upstream.

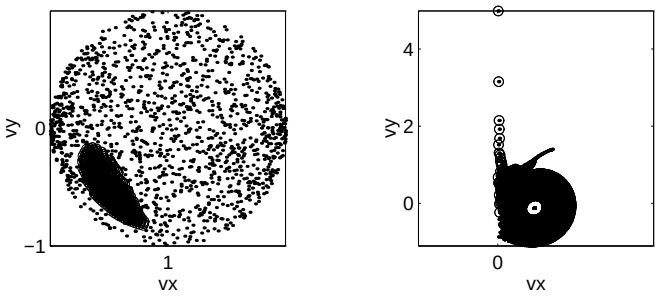

(a) (b)

Fig. 6. Incident pick up ion distribution and multiply reflected ions (a) at the edge of the foot $x = -0.3(V_u/\Omega_u)$ (multiply reflected ions fill the black area) and (b) near the ramp $x = -0.005v_u/\Omega_u$ (multiply reflected ions shown by circles).

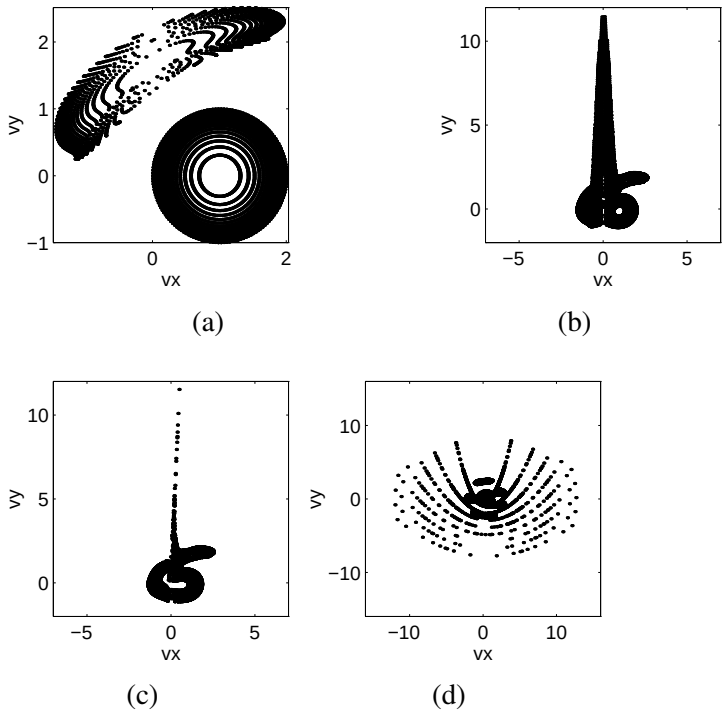

Fig. 7. Pickup ion velocity space distribution at the high Mach number $M = 7.5$ perpendicular shock with the ramp with $D_r = 0.01(V_u/\Omega_u)$ (a) in the upstream region $x = -0.6(V_u/\Omega_u)$, (b) at the upstream edge of the ramp $x = -0.005(V_u/\Omega_u)$, (c) at the downstream edge of the ramp $x = 0.005(V_u/\Omega_u)$, and (d) far downstream at $x = 5(V_u/\Omega_u)$.

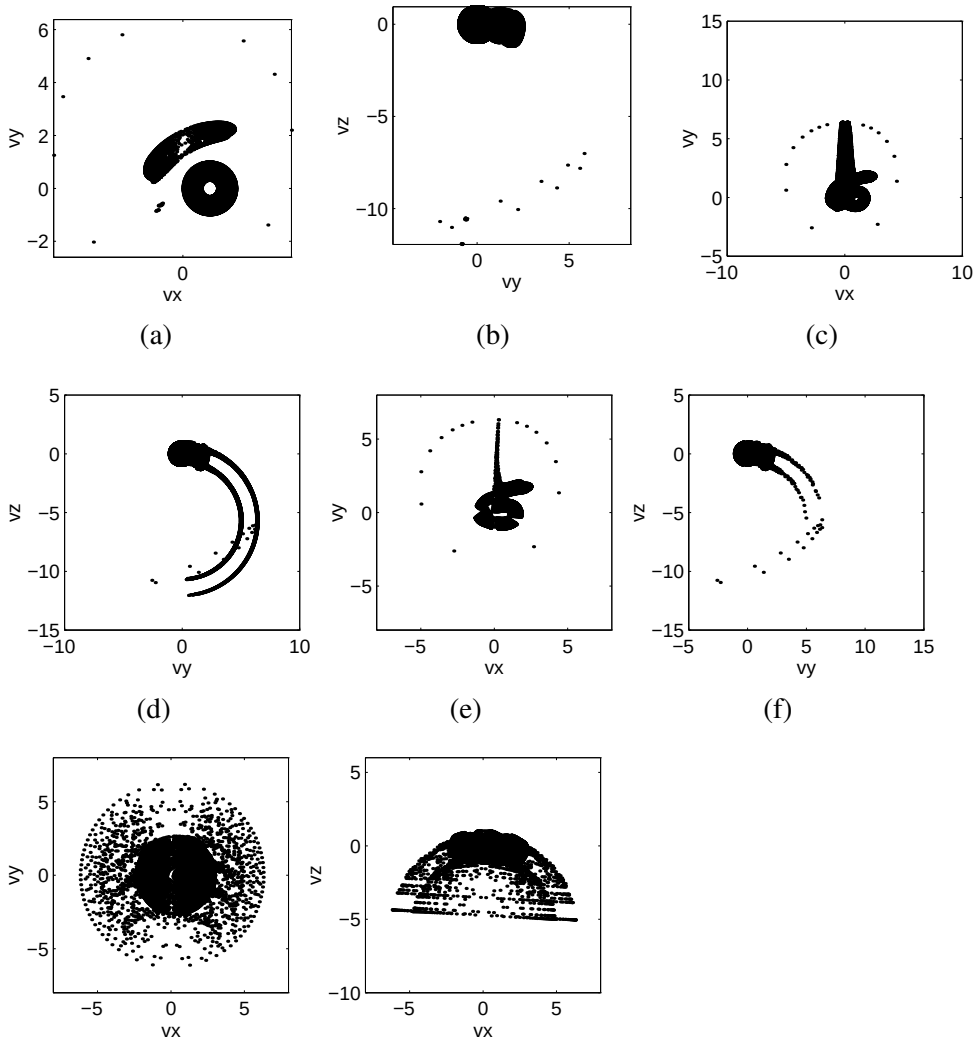

Fig. 8. Pickup ion velocity space distribution at the high Mach number $M = 7.5$ quasi-perpendicular shock $\theta_{Bnu} = 80^\circ$ with the ramp width $D_r = 0.01(V_u/\Omega_u)$, at the same positions as in Figure 7: (a) and (b) in the upstream region, (c) and (d) at the upstream edge of the ramp, (e) and (f) at the downstream edge of the ramp, and (g) and (h) far downstream.

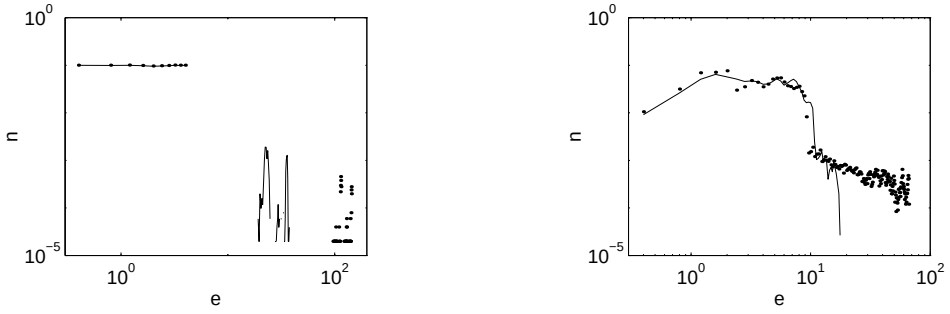

(a) (b)

Fig. 9. Pickup ion spectrum in the far upstream region (a) at $x = -5(V_u/\Omega_u)$ and (b) far downstream at $x = 5(V_u/\Omega_u)$ for $\theta_{Bn} = 80^\circ$ (dotted line) and $\theta_{Bn} = 70^\circ$ (solid line). Width of the ramp is $0.01(V_u/\Omega_u)$

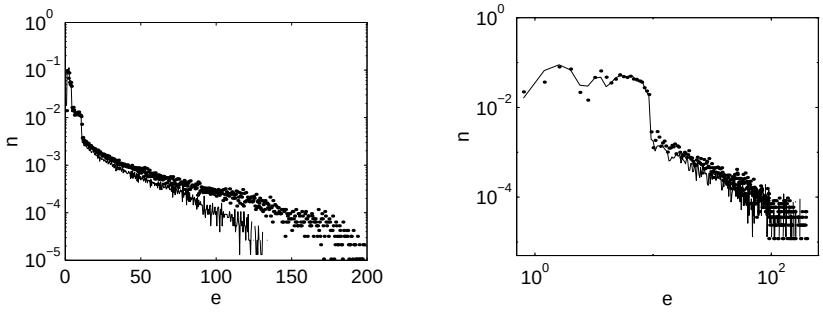

(a) (b)

Fig. 10. Pickup ion spectrum (a) at the upstream edge of the ramp $x = -D_r/2$ and (b) far downstream at $x = 5(V_u/\Omega_u)$, at the super-critical $M = 7.5$ perpendicular shock for the total cross-shock potential $\varphi = 0.7(m_i V_u^2/2)$ (dotted line) and $\varphi = 0.5(m_i V_u^2/2)$ (solid line). The ramp width is $D_r = 0.01(V_u/\Omega_u$.

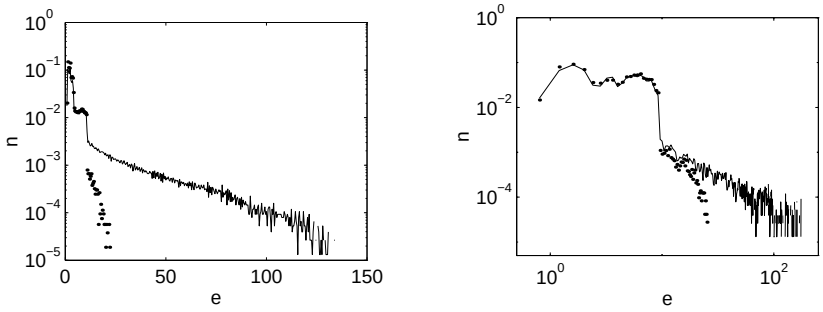

Fig. 11. Pickup ion spectrum before the ramp $x = -D_r/2$ (a) and in far downstream region $x = 5v_u/\Omega_u$ (b) at the super-critical $M = 7.5$ perpendicular shock with the ramp width $D_r = 0.01(V_u/\Omega_u)$ (solid line) and $D_r = 0.03(V_u/\Omega_u)$ (dotted line). The cross-shock potential is $\varphi = 0.5(m_i V_u^2/2)$

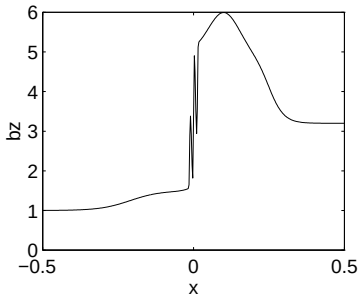

(a)

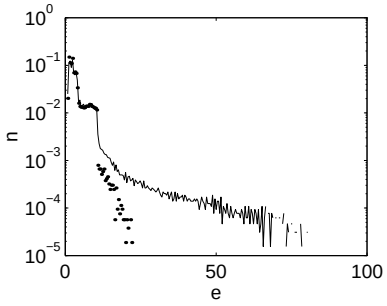

(b)

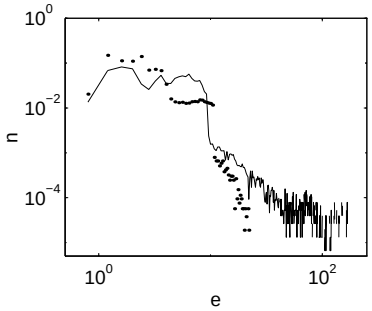

(c)

Fig. 12. Pickup ion spectrum before the ramp $x = -D_r/2$ (b) and far downstream at $x = 5(V_u/\Omega_u)$ (c) at the super-critical $M = 7.5$ perpendicular shock without (dotted line) and with (solid line) a substructure in the magnetic field profile the super-critical $M = 7.5$ perpendicular shock without (dotted line) and with (solid line) a substructure in the magnetic field profile (shown in subfigure (a)). The width of the ramp is $D_r = 0.03(V_u/\Omega_u)$.

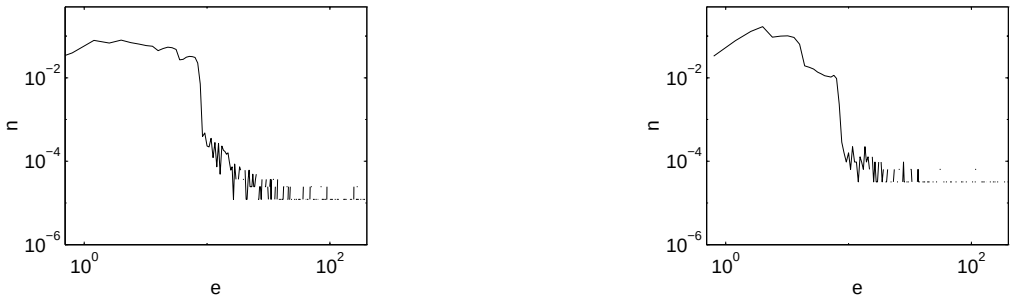

(a) (b)

Fig. 13. Downstream spectra of heavy accelerated pickup ions (a) $m_i = 4m_p$, and (b) $m_i = 16m_p$, at the super-critical $M = 7.5$ perpendicular shock with the ramp width $D_r = 0.01(V_u/\Omega_u)$. The cross-shock potential is $\varphi = 0.5(m_i V_u^2/2)$